In Situ Burning via Towed Boom of Oil Spilled at Sea

by

George Carrier, Francis Fendell, and Jay Mitchell
Center for Propulsion Technology and Fluid Mechanics
TRW Space & Technology Group, Redondo Beach, CA 90278

Operational guidance for the efficient use of combustion in the cleanup of a surface oil film, formed as a result of a spill at sea, is sought by approximate analysis. In remediation by burning, the spilled oil itself provides the energy for its cleanup. Attention is focused on situations holding relatively far from the source of the spill and/or relatively long after the spill: the oil is taken to have so dispersed that the thickness of the film is on the order of a few millimeters. Under such conditions, the oil film is unlikely to burn without the use of multiple towed booms, each boom spreading its already-ignited, localized fire to continuously collected, previously unignited portions of the oil film. A simple, quasisteady, two-dimensional analysis suggests efficient values for the tow speed and the tow-line length as functions of such parameters as the oil density, oil-film thickness, oil burn/evaporation rate, etc. The analysis leads to specific suggestions for apparently unreported laboratory experiments that may be informative prior to at-sea operation.

INTRODUCTION

We consider an option for the removal of oil spilled at sea. The option includes containment by towed booms and combustion of the oil (Fig. 1) [1-7]. It seems unlikely that the formation of soot and other hydrocarbon products [3,4,8], for which there may be methods of mitigation [9,10], could outweigh the advantage of this in situ reduction (even elimination) of the oil. Alternative methods that remove, as distinguished from redistribute and/or disperse, the spilled oil entail large requirements for collection, storage, transportation, and disposal [1].

Accordingly, we analyze the fluid dynamics (including the consequences of mass conservation) of the combustion phenomena in order to obtain estimates of suitable operational parameters.

We note that extensive modeling, experiments, and observations are available concerning the spreading and fate of oil spilled at sea in the absence of countermeasures [11-13].

THE DYNAMICS OF THE OIL LAYER

We adopt a two-dimensional idealization of the real three-dimensional configuration (Fig. 1). As is shown in Fig. 2, we fix our coordinates in the boom so that the flow (relative to the boom, of course) is in the x direction and is independent of time.

Environment Canada. Arctic and Marine Oilspill Program Technical Seminar, 15th. June 10-12, 1992, Edmonton, Canada, Environment Canada, Ottawa, Ontario, 659-680 pp, 1992.

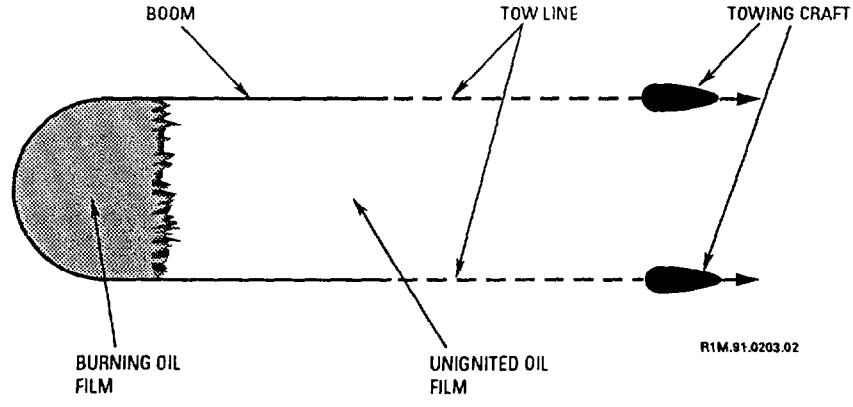

Figure 1. Plan view, not to scale, of a typical oil-film-"herding"-and-burning operation at sea, including a towed U-configured boom.

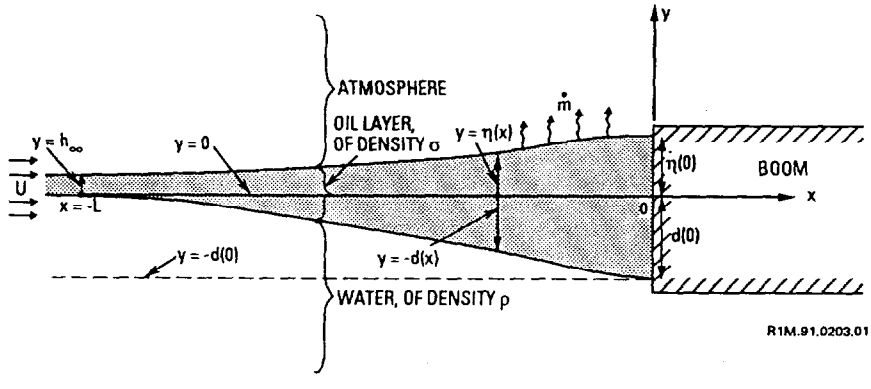

Figure 2. Schematic for a quasisteady, two-dimensional model of the burning [with oil-surface-regression rate $\dot{m}(x)$, typically on the order of 0.1 mm/s] of an oil slick of ambient thickness h_∞ and of density σ. In the frame of reference of a towed impervious boom, the ambient oil and water at $x \leq -L$ approach at the towing speed U.

The vertical coordinate, y, has its origin at the altitude of the oil-water interface upstream of the burning region, which is adjacent to the boom. For operating parameters of interest, the oil layer is very thin compared with the range of x over which the dynamics are at issue, and thus the slope of both the oil-atmosphere surface, $y = \eta(x)$, and the oil-water interface, $y = -d(x)$, is very small. It is consistent with the foregoing to adopt a hydrostatic approximation for the vertical-momentum balance. We use the notation indicated in Fig. 2, so that the equation which represents this approximation of the vertical-momentum balance is (g is the magnitude of the gravitational acceleration)

$$p_y + \sigma g = 0 \quad \text{in} \quad -d(x) < y < \eta(x) \ . \tag{1}$$

Here σ is the density of the oil and the datum of the pressure p is taken as follows:

$$p = 0 \text{ at } y = \eta(x) \ . \tag{2}$$

It follows that

$$p(x,y) = \sigma g[\eta(x) - y], \quad \text{in} \quad -d(x) < y < \eta(x) \ , \tag{3}$$

and

$$p_x = \sigma \, g\eta'(x), \quad \text{in} \quad -d(x) < y < \eta(x) \ . \tag{4}$$

It is also consistent with the foregoing to ignore the horizontal acceleration of the oil so that (with μ_o denoting the dynamic viscosity of the oil)

$$p_x = \mu_o \, u_{yy} \ . \tag{5}$$

Since p_x is independent of y from Eq. 4, u is quadratic in y. The (almost horizontal) velocity of the oil-water interface at $y = -d(x)$ is denoted by $u_1(x)$. The velocity gradient in the vertical direction, $u_y(x,y)$, must vanish at $y = \eta(x)$, and therefore

$$u(x,y) = u_1(x) - \frac{\sigma g \eta'(x)}{2\mu_o} [y + d(x)][d(x) + 2\eta(x) - y] \ . \tag{6}$$

Mass conservation in $-L < x < 0$, $-d(x) < y < \eta(x)$, where $\eta'(x) = 0$ for $x \leq -L$, is given by

$$u_x + v_y = 0 \ . \tag{7}$$

Since $u(0,y) = 0$ because the boom is impervious,

$$\frac{d}{dx} \int_{-d(x)}^{\eta(x)} u(x,y) \, dy - [\eta'(x)] \, u[x,\eta(x)] + d'(x) \, u[x,-d(x)]$$

$$+ v[x,\eta(x)] - v[x,-d(x)] = 0, \tag{8}$$

or

$$\int_{-d(x)}^{\eta(x)} u(x,y)\, dy = \int_{x}^{0} \dot{m}(\delta)\, d\delta \ , \tag{9}$$

since

$$v(x,\eta) - [u(x,\eta)]\, \eta'(x) = \dot{m}(x),$$

$$v(x,-d) - [u(x,-d)]\, d'(x) = 0 \ , \tag{10}$$

and $\dot{m}(x)$ is the vertical efflux of the pyrolyzing oil (with the dimensions of a velocity). The upstream edge of the combustion zone is at $x = -L$. The result given by Eq. 9 may seem immediately self-evident, but the development assists the exposition.

Somewhat varying empirical data regarding the consumption rate of an oil film on water have been published [3,6,11-14]. More data are needed concerning the dependence of the oil burning rate on layer thickness, type of oil, and wind speed if the model results are to be definitive; this subject is briefly readdressed below.

If the integral on the right-hand side of Eq. 9 is denoted $M(x)$, then mass conservation [i.e., Eq. 9] implies $M(-L) = [u_1(-L)][\eta(-L)]$, since $u(-L,y) = u_1(-L)$ and $d(-L) = 0$ by definition. Substitution of Eq. 6 in Eq. 9 gives

$$(\eta + d)\, u_1 - \frac{\sigma g \eta'}{3\mu_o} (\eta + d)^3 = M(x) \ . \tag{11}$$

We collect some of the above, append several bits of notation, and add some simple consequences of the foregoing analyses of the oil layer:

$$p[x,-d(x)] = \sigma g(\eta + d) \ , \tag{12}$$

$$\tau_{xy}[x,-d(x)] \equiv \mu_o\, u_y[x,-d(x)] = -[\sigma g \eta'(x)][d + \eta] \ , \tag{13}$$

$$u_1(-L) \equiv U \ , \tag{14}$$

$$\eta(-L) \equiv h_\infty \ , \tag{15}$$

and

$$d(-L) = 0 \ . \tag{16}$$

THE DEEP-WATER DYNAMICS

The motion in the deep water, i.e., the perturbation in velocity from its upstream horizontal value, U, is driven by the friction that the oil exerts on the water at the oil-water interface. We can expect with confidence that the perturbation

velocity is not greater than U itself. Accordingly, the "Bernoulli correction" to the hydrostatic pressure in the water can be no larger than that in the oil. It is thereby consistent with the analysis of the previous section (wherein the Bernoulli corrections were ignored) to adopt an Oseen approximation [18] to the dynamic balance, and to locate the oil-water interface at a depth that is consistent with the considerations set forth in this paragraph and with

$$\frac{\partial p}{\partial y} = -\rho g \quad \text{in} \quad y < -d(x) \ , \tag{17}$$

where ρ denotes the density of the water. Thus, in $y \leq -d(x)$ and in $x \leq -L$, the pressure in the water, p_{water}, is given by

$$p_{water}(-L,y) = \sigma g h_\infty - \rho g y \ . \tag{18}$$

But

$$p_{water}(x,y) = \sigma g[\eta(x) + d(x)] - \rho g(y + d) \ . \tag{19}$$

Equating the two expressions gives

$$\eta = \frac{\rho - \sigma}{\rho} (\eta + d) + \frac{\sigma h_\infty}{\rho} \ , \tag{20}$$

and

$$\eta' = \frac{\rho - \sigma}{\rho} (\eta + d)' \ . \tag{21}$$

The appropriate Oseen model for the perturbation velocity u^* is (since $u_{xx} \lll u_{yy}$)

$$\mu u^*_{yy} - \frac{\rho U}{3} u^*_x = 0 \quad \text{in } y < 0 \ , \tag{22}$$

where μ denotes the viscosity of the water, and since $u^*(x,y) \equiv u(x,y) - U$,

$$u^*(x,0) = u_1(x) - U \ . \tag{23}$$

In this formulation we use the usual small-surface-slope approximation wherein (in the notation of this problem) $u^*[x,-d(x)]$ is replaced by $u^*(x,0)$. The choice of the effective convective speed (U/3) in the linearized convective operator of Eq. 22 is standard and well-motivated [18]. Also, in this treatment of the dynamics of the water, we extend the domain to encompass $y < 0$ and $-\infty < x < \infty$. We defer until later the adjustment that will be necessary in order to accommodate the requirement that $u^*(0,0) = -U$, since $u_1(0) = 0$ because we expect that the oil-water interface intersects the impervious boom (Fig. 2).

The Fourier transform in the coordinate x of Eq. 22 is

$$\mu \bar{u}^*_{yy}(\varsigma,y) - \frac{\rho U i \varsigma}{3} \bar{u}^*(\varsigma,y) = 0 , \tag{24}$$

where ς is the transform variable and a super bar signifies a transformed quantity. By the requirement of boundedness, and by use of Eq. 23 to identify the function of integration, solution of Eq. 24 gives

$$\bar{u}^*(\varsigma,y) = \left[\bar{u}_1(\varsigma) - \frac{U}{i\varsigma}\right] \exp\left\{\left[\frac{\rho U}{3\mu} i\varsigma\right]^{1/2} y\right\} . \tag{25}$$

The stress τ_{xy} is given at y = 0 by

$$\tau_{xy}(x,0) = \mu u_y(x,0) , \tag{26}$$

and its Fourier transform in x is, by Eq. 25,

$$\bar{\tau}_{xy} \equiv \bar{\tau}(\varsigma) = u\left(\frac{\rho U i\varsigma}{3\mu}\right)^{1/2} \left[\bar{u}_1(\varsigma) - \frac{U}{i\varsigma}\right] . \tag{27}$$

Inversion of Eq. 27, by use of convolution, gives, in view of Eq. 14,

$$u_1(x) - U = \left(\frac{3}{\rho\mu U}\right)^{1/2} \int_{-L}^{x} \frac{\tau_{xy}(x_1)}{[\pi(x - x_1)]^{1/2}} dx_1 . \tag{28}$$

THE MATHEMATICAL PROBLEM

We now define the following dimensionless variables:

$$w(s) \equiv \frac{u_1(x)}{U} , \quad H(s) \equiv \frac{\eta(x) + d(x)}{h_\infty} , \quad f(s) \equiv \frac{M(x)}{Uh_\infty} ; \tag{29}$$

$$s \equiv \frac{x}{L} , \quad \lambda \equiv \frac{\rho - \sigma}{\rho} \frac{g h_\infty^3}{3UL\mu_0/\sigma} , \quad K \equiv \frac{\sigma(\rho - \sigma)}{\rho^2} \frac{g h_\infty^2}{(\nu U^3 L/3)^{1/2}} , \tag{30}$$

where $\nu \equiv \mu/\rho$. The presence of the quantities U and L as multiplicative factors in the denominators of the parameters λ and K is noteworthy.

By use of Eqs. 13, 21, 26, 29, and 30, we may rewrite Eqs. 11 and 28 as

$$\lambda H^3(s)\, H'(s) = w(s)\, H(s) - f(s) , \tag{31}$$

and

$$w(s) - 1 = -K \int_{-1}^{s} \frac{H(s_1)\, H'(s_1)}{[\pi(s - s_1)]^{1/2}}\, ds_1 \ . \tag{32}$$

The dimensionless dependent variables w and H must obey the conditions

$$H(-1) = w(-1) = 1 \ . \tag{33}$$

In the absence of pyrolysis and burning, f(s) = 1; then, w(s) = H(s) = 1, i.e., the volumetric flux per length Uh_∞ accumulates at the boom (and soon overruns and underruns it). There are two more constraints on the system. First, the upstream edge of the combustion zone must proceed to the left (in the natural coordinate system) at speed U. Thus, the operating speed U must be chosen in accord with the firespread rate of the oil layer, which, in turn, depends on the thickness of the layer, the wind speed, properties of the oil, and possibly other factors. Little is known about the firespread rate [3], and data are needed before one can exploit any model of the oil-slick-burning phenomenon. Second, for consistency with Fig. 2, it is also necessary that w(0) = 0.

For some values of λ and K, it is a remarkable coincidence that w(0) does become zero. For other cases one must note that the analysis fails in a very small neighborhood of s = 0. It is also evident, however, that in so small a region, any adjustment that the velocity field requires can perturb only very locally the overall balance for either the mass or momentum of the oil. Figure 3 is a schematic diagram of the perturbed geometry that would accompany the flow for those values of λ and K for which Eqs. 31 and 32 do not yield w(0) = 0, upon integration from s = -1 to s = 0.

Incidentally, for the convenience of treating only positive values of the independent variable, we sometimes elect to adopt the coordinate t, where

$$t = s + 1, \quad \text{so} \quad 1 \geq t \geq 0 \ . \tag{34}$$

However, we refer to the primary dependent variables as H and w whether we work in the s or t coordinate, because we seek to avoid further proliferation of notation.

Once solution for H(t) is obtained from Eqs. 31-32, $\eta(x)$ is available from Eq. 20, and d(x) follows by subtraction, from the middle relation of Eq. 29.

We concentrate below entirely on the case of a pyrolyzation rate uniform in the domain $1 \geq t \geq 0$, so f(t) = 1 - t for calculations reported here. Again, obtaining further data seems desirable before pursuing alternative distributions [though in all distributions of interest f(t) = 1 for t = 0 and f(t) = 0 for t = 1].

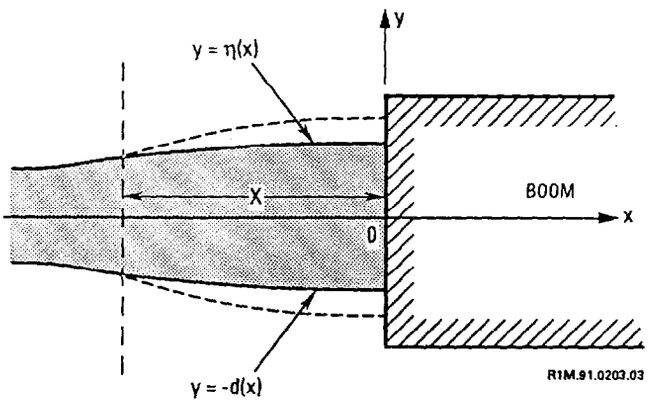

Figure 3. The solid curves delineate the limits of the (shaded) oil layer, $y = \eta(x)$ and $y = -d(x)$, as given by the integration of Eqs. 31-33. When, according to the model, the horizontal velocity component at the oil-water interface exceeds zero at the boom, $x = 0$, then over a distance X, which can be only a few multiples of the vertical expanse $[\eta(0) + d(0)]$ and which is much less than the distance L (Fig. 2), there is a boundary-layer-like modification (not analyzed) such that each of $\eta(x)$ and $d(x)$ is given by its respective dashed-curve counterpart.

SOLUTION

We proceed to identify, by numerical solution, those values of the dimensionless groups λ and K for which practically interesting behavior is obtained. Such behavior is characterized by (1) H increasing monotonically as t increases, such that the value of H at the boom is at least a few multiples of the value of H at $t = 0$; and (2) w decreasing monotonically as t increases, preferably such that w is close to zero at the boom. Then, for practically interesting values of the parameters ρ (water density), σ (oil density), h_∞ (ambient oil-film thickness), μ_0 (dynamic water viscosity), and ν (kinematic water viscosity), via Eq. 30 we infer values for U (tow speed) and L (burning-patch length) from the adopted values of λ and K.

Alternatively, and more directly, we can adopt values for U and L (as well as for ρ, σ, h_∞, μ_0, and ν), and thus specify values of λ and K. In choosing values, we recall [from Eqs. 29-30, the definition of M(x) given above Eq. 11, and Eq. 34] that the value of the regression speed $\dot{m}$, such that previously herded oil leaves the layer as fast as freshly herded oil enters the layer (so a steady configuration persists), is given by

$$\dot{m} = \frac{dM}{dx} = \frac{Uh_\infty}{L}\frac{df}{dt} \to -\frac{Uh_\infty}{L} \qquad (35)$$

for $f(t) = 1 - t$. Equation 35 guides the parameter assignments for consistency with oil-layer-burning rate data: according to [6], typically $\dot{m} \simeq 0.06 - 0.07$ mm/s, and according to [5], $\dot{m} \simeq 0.035 - 0.05$ mm/s. We need to ascertain that the system, Eqs. 31-33, has solutions with the desired properties for the values for the groups λ and K implied by the parameter assignments.

We now discuss details of the calculations. From knowledge of $H(t)$ and $w(t)$, from Eq. 31 we compute $H(t + \Delta t)$, where Δt is a very small increment, by holding w fixed at the value $w(t)$, e.g., by the standard fourth-order Runge-Kutta formula; with H known over the $(t, t + \Delta t)$ interval, we then obtain $w(t + \Delta t)$ from a trapezoidal-rule-type integration of Eq. 32. We then repeat the two-step cycle for the next incremental interval in t. We search for a Δt small enough that the overall results are effectively invariant to the step size Δt, rather than iterate for every increment in the independent variable t. For the calculations reported below, $\Delta t = 0.0001$. Incidentally, the integrably singular kernel $K(s - s_1) \equiv [\pi(s - s_1)]^{-1/2}$ in Eq. 32 may be conveniently and accurately modified this:

$$K(s) = \begin{cases} a - bs - cs^2, & 0 \leq s \leq s_o \\ (\pi s)^{-1/2}, & s_o \leq s \leq 1, \end{cases} \tag{36}$$

where requiring the continuity of value and slope at s_o ($\ll 1$) and requiring the equality of the integrals

$$\int_0^{s_o} (a - bs - cs^2)\, ds = \int_0^{s_o} (\pi s)^{-1/2}\, ds \tag{37}$$

imply

$$a = \frac{15}{4\pi\, s_o^{1/2}}, \quad b = \frac{5}{\pi^{1/2}\, s_o^{3/2}}, \quad c = \frac{9}{4\pi^{1/2}\, s_o^{5/2}}. \tag{38}$$

Also, we note that, since $H'(0) = w'(0) = 0$, for $f(t) = 1 - t$, as $t \to 0$, from Eqs. 31-38,

$$H(t) \simeq 1 + \lambda^{-1}\, t^2/2 + \ldots, \quad w(t) = 1 - Kat^2/(2\lambda) - \ldots. \tag{39}$$

Thus, although the solution of Eq. 31 superficially might seem to possess boundary-layer character for $1 \gg \lambda \geq 0$, in fact, the right-hand side vanishes at $t = 0$, in view of Eq. 33 and in view of the constraint that (at $t = 0$) $f(0) = 1$ by definition; that is, the solution of the reduced equation satisfies the boundary conditions. In fact, as $t \to 1$ and $f(t) \to 0$, the left-hand side of Eq. 31 tends to balance the first term on the right-hand side, since in general the value of $w(1)$ given by Eqs. 31 and 32 is small but finite. If $w(1) \to 0$, from Eq. 32,

$$K \to \left\{ \int_0^1 \frac{H(t_1)\, H'(t_1)}{\left[\pi(1 - t_1)\right]^{1/2}} \, dt_1 \right\}^{-1} , \tag{40}$$

so it is not implausible that we find that H is larger as $t \to 1$ for smaller values of the parameter K, for fixed values of λ. As λ is increased for fixed K, typically we find that w(t) decreases less as t increases from zero to unity.

The nominal parameter assignments are taken to be as follows [5]:

$$\nu = 0.01 \text{ cm}^2/\text{s} , \quad \rho = 1 \text{ g/cm}^3 , \quad g = 980 \text{ cm/s}^2 ,$$

$$h_0 = 0.2 \text{ cm} , \ \mu_0 = 1 \text{ g/(cm s)} , \ \sigma = 0.934 \text{ g/cm}^3 ,$$

$$U = 26 \text{ cm/s} , \ L = 1500 \text{ cm}. \tag{41}$$

These assignments imply that the nominal values of λ and K are:

$$\lambda = 4.13 \times 10^{-6} , \ K = 8.15 \times 10^{-3} , \ \dot{m} = -3.47 \times 10^{-3} \text{ cm/s} . \tag{42}$$

In results reported here, all parameters taken on their nominal values in the absence of explicit statement to the contrary, and the independent variable is taken to be t. For the nominal case $H(1) \doteq 17.8$, $w(1) \doteq 0.01$. Figure 4 presents results for w(t) for the following cases:

(1), nominal case [see Eqs. 41 and 42];

(2), $U = 52$ cm/s, $\lambda = 2.06 \times 10^{-6}$, $K = 2.88 \times 10^{-3}$,

$\dot{m} = -6.93 \times 10^{-3}$ cm/s ;

(3), $L = 750$ cm, $\lambda = 8.26 \times 10^{-6}$, $K = 1.15 \times 10^{-2}$,

$\dot{m} = -6.93 \times 10^{-3}$ cm/s ;

(4), $h_\infty = 0.4$ cm, $\lambda = 3.30 \times 10^{-5}$, $K = 3.26 \times 10^{-2}$,

$\dot{m} = -6.93 \times 10^{-3}$ cm/s ;

(5), $\sigma = 0.82 \frac{g}{cm^3}$, $\lambda = 9.89 \times 10^{-6}$, $K = 1.95 \times 10^{-2}$,

$\dot{m} = -3.47 \times 10^{-3}$ cm/s;

and

(6), $\mu_o = 2.0 \frac{g}{cm\ s}$, $\lambda = 2.06 \times 10^{-6}$, $K = 8.15 \times 10^{-3}$,

$\dot{m} = -3.47 \times 10^{-3}$ cm/s. (43)

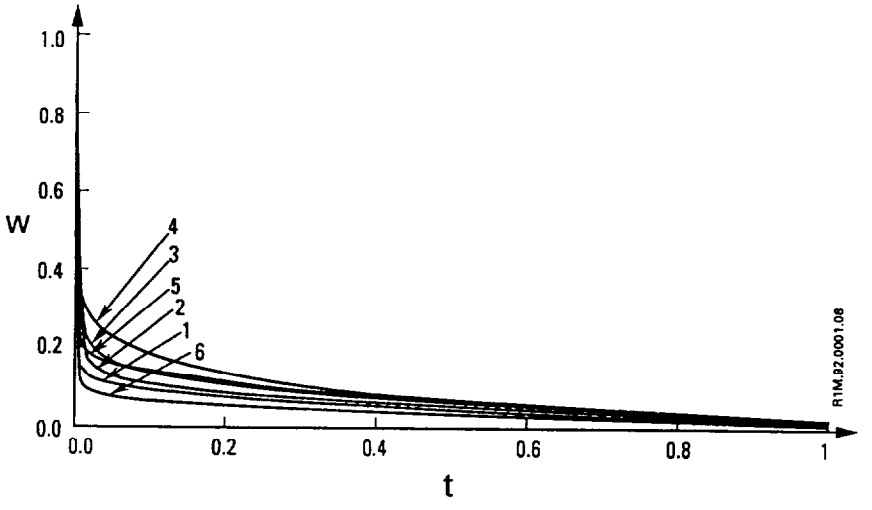

Figure 4. The normalized oil-water-interface speed w as a function of the nondimensional spatial coordinate t, for the cases of Eq. 43.

Figure 5 presents the corresponding results for H(t) for the cases of Eq. 43. Figure 6 presents results for w(t) for most of the following cases, for all of which $\dot{m} = -3.47 \times 10^{-3}$ cm/s, the nominal value:

(1), nominal case [see Eqs. 41 and 42];

(7), U = 52 cm/s , L = 3000 cm, $\lambda = 1.03 \times 10^{-6}$,

$K = 2.04 \times 10^{-3}$;

(8), U = 13 cm/s , L = 750 cm, $\lambda = 1.65 \times 10^{-5}$,

$K = 3.26 \times 10^{-2}$;

(9), U = 52 cm/s , h_∞ = 0.1 cm, $\lambda = 2.58 \times 10^{-7}$,

$K = 7.20 \times 10^{-2}$;

(10), $U = 13$ cm/s , $h_\infty = 0.4$ cm, $\lambda = 6.61 \times 10^{-5}$,

$K = 9.22 \times 10^{-2}$;

(11), $h_\infty = 0.4$ cm , $L = 3000$ cm, $\lambda = 1.65 \times 10^{-5}$,

$K = 2.30 \times 10^{-2}$; and

(12), $h_\infty = 0.1$ cm , $L = 750$ cm, $\lambda = 1.03 \times 10^{-6}$,

$K = 2.88 \times 10^{-3}$. (44)

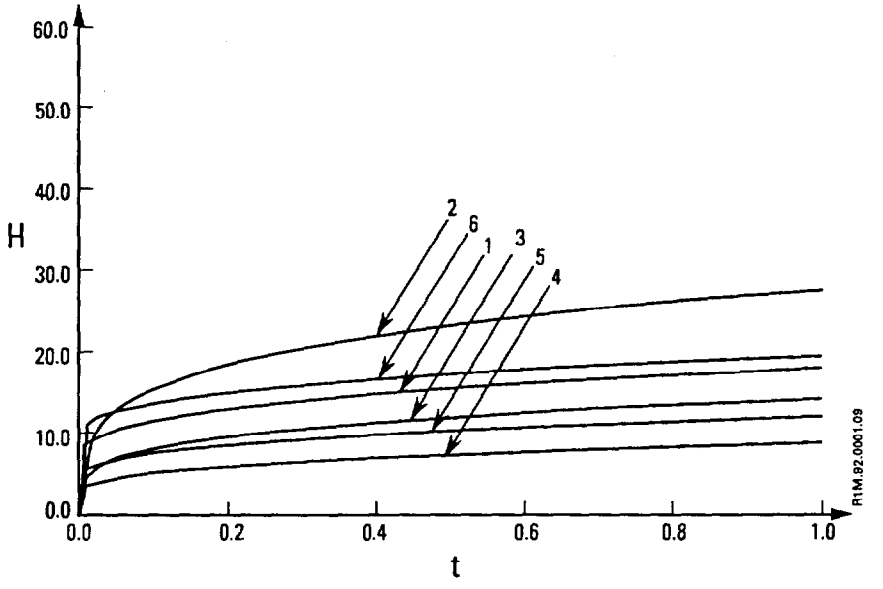

Figure 5. The dimensionless oil-layer thickness H as a function of the nondimensional spatial coordinate t, for the cases of Eq. 43.

Figure 7 presents the corresponding results for H(t) for most of the cases of Eq. 44. The rather well-defined front of the towed-boom-thickened region, and the oil thickness at the boom (often several centimeters for a millimeter-thick oil film), are noteworthy. Because the length of the boom-thickened oil layer L is typically 1.5 m or more, the maximum compressional-strain rate for $u_1(x)$ is $O(1/s)$. Figure 8, which identifies the location in (K,λ) space of the dozen cases just enumerated, suggests the dimensionless-parameter ranges of particular physical interest.

It is worth noting that for some combinations of parameter values, the numerical results suggest that the operation may be unsatisfactory, because the operation is ineffective and/or unstable

[e.g., H(t) barely exceeds unity at t = 1 and/or w(t) goes to zero for t < 1 and/or highly oscillatory behavior of H(t) or w(t) occurs].

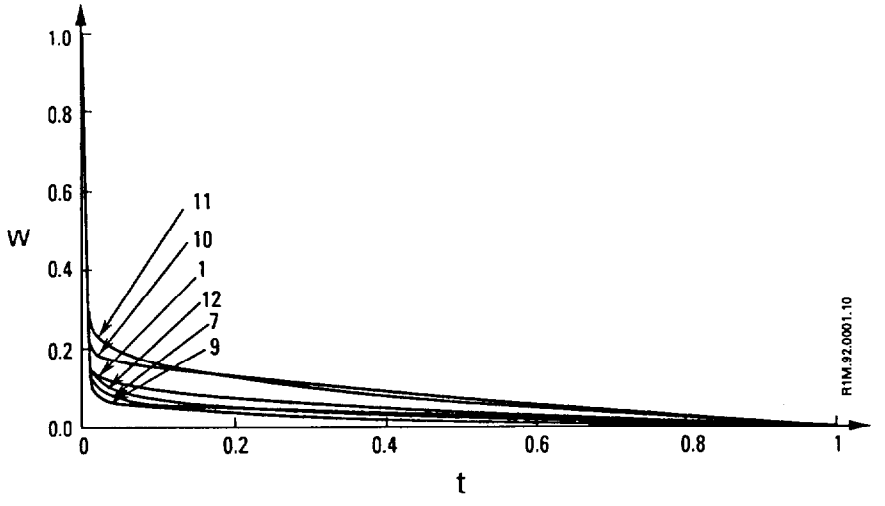

Figure 6. Same as Fig. 4, but for most of the cases of Eq. 44.

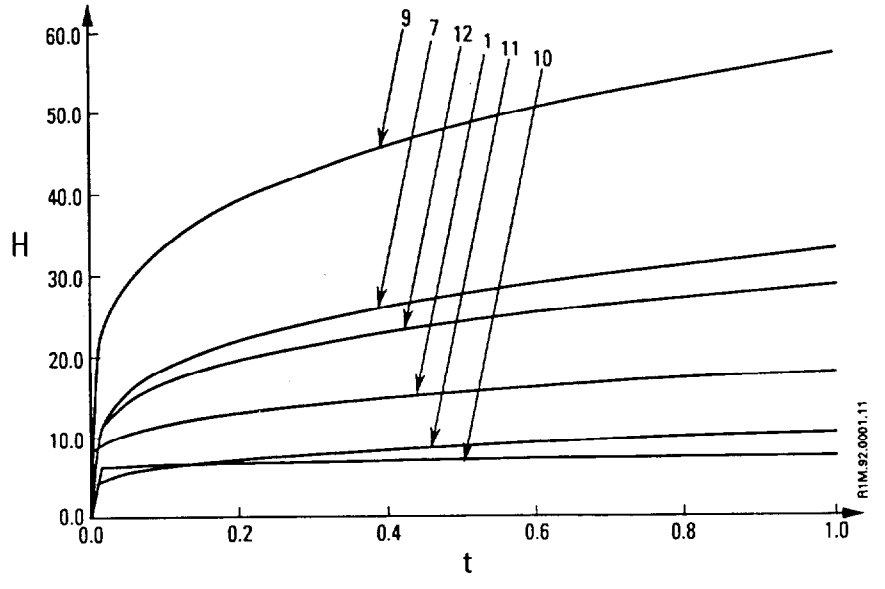

Figure 7. Same as Fig. 5, but for most of the cases of Eq. 44.

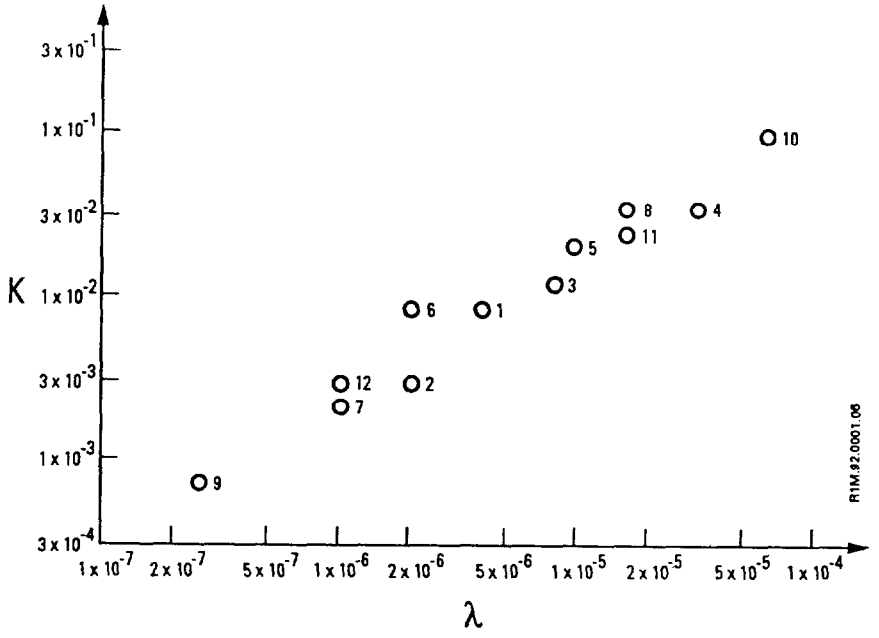

Figure 8. Identification in (K,λ) space of the twelve illustrative cases specified by Eqs. 41-44. The combinations of dimensionless parameters which comprise the dimensionless groups K and λ are defined in Eq. 30.

BOOM CONFIGURATION

To this point, we have carried out a one-dimensional analysis of an oil-herding-and-burning operation, taken to be quasisteady in the frame of reference fixed in the (towed) boom. Here we examine more closely the configuration taken on by the boom, described above simply as U-shaped. We model the boom as a uniform flexible string, which supports no compression or shearing stress or bending moment, so that the force exerted at any point in the string can be only a tension T directed along the tangent to the string at that point (Figs. 9 and 10) [19]. The distance s^* is the arc length measured along the string from the point of symmetry (taken to be the origin of a Cartesian coordinate system fixed in the boom: $x^* = y^* = 0$). The super asterisk is present to distinguish the present usage of some conventional symbols from our earlier usage of the same symbols for other designations. The towing is taken to be such that the y^* axis is an axis of symmetry.

If D denotes the fluid-dynamic drag on the towed boom owing to the flow U, then the balance of forces locally normal to the boom gives (C_D, the drag coefficient, is approximately unity for the range of the Reynolds number of practical interest [20], and H* is depth of the wetted part of the boom):

$$T\, d\theta = D\, ds^* = (\rho/2)\, C_D (U \cos\theta)^2\, H^*\, ds^* \; ; \tag{45}$$

$$\frac{d\theta}{ds^*} = \frac{\rho C_D\, U^2\, H^*}{2T} \cos^2\theta, \text{ so } \tan\theta = ks^* \tag{46}$$

by symmetry, provided that T is a constant and

$$k \equiv \rho C_D\, U^2\, H^*/(2T) \; .$$

However, dT/ds* is equal to the drag locally tangential to the string, and, since this drag is negligible, T is indeed constant. If L* is half the length of the boom, then

$$\tan\theta_0 = kL^* \; , \tag{47}$$

where ρ, C_D, U^2, H*, and L* are taken as known. While the tension T is not taken as given, the towing vessels must continue to pull in a fixed direction θ_0 to keep the boom configuration unchanged in time.

Since $(dy^*/dx^*) = \tan\theta$ and $(ds^*)^2 = (dx^*)^2 + (dy^*)^2$,

$$\frac{dx^*}{ds^*} = \cos\theta = \left(1 + k^2\, s^{*2}\right)^{-1/2} \; ,$$

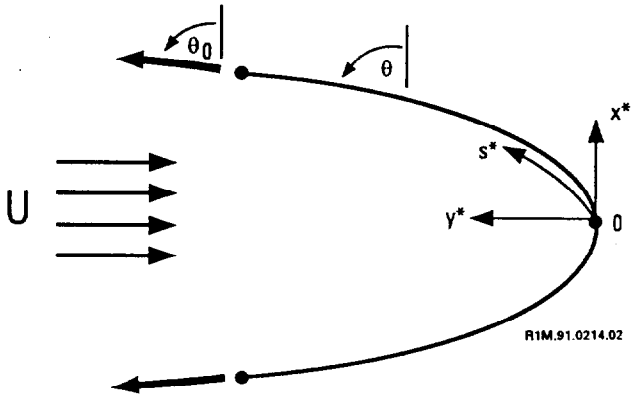

Figure 9. Sketch of the coordinate systems used in examining the boom configuration for herding and burning an oil film on water.

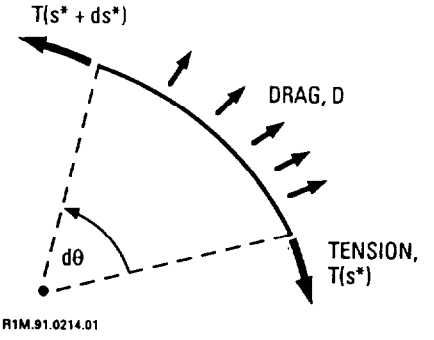

Figure 10. Sketch of the force balance used in examining the boom configuration for herding and burning an oil film on water.

$$\frac{dy^*}{ds^*} = \sin\theta = ks^*/\left(1 + k^2 s^{*2}\right)^{1/2} . \tag{48}$$

Hence, with $L^* \geq s \geq 0$,

$$x^*(s^*) = k^{-1} \ln\left[ks^* + \left(1 + k^2 s^{*2}\right)^{1/2}\right] ,$$

$$y^*(s^*) = k^{-1}\left[\left(1 + k^2 s^{*2}\right)^{1/2} - 1\right] . \tag{49}$$

From Eqs. (47) and (49),

$$x^*(L^*) = \frac{L^*}{\tan\theta_o} \ln\left(\tan\theta_o + \sec\theta_o\right) ,$$

$$y^*(L^*) = \frac{L^*}{\tan\theta_o} \left(\sec\theta_o - 1\right) . \tag{50}$$

For $[(\pi/2) - \theta_o] \equiv \epsilon$, where $0 < \epsilon \ll 1$, i.e., for the case in which the two craft tow slightly divergently from a parallel alignment, $x^*(L^*) \simeq L^*\epsilon \ln(2/\epsilon)$ and $y^*(L^*) \simeq L^* - O(\epsilon L^*)$. More generally, from Eq. 50, for assigned θ_o and L^*, the separation distance $x^*(L^*)$ is inferred; alternatively, for assigned $x^*(L^*)$ and L^*, the towing angle θ_o is inferred. The parameter k follows from Eq. 47, so the entire boom configuration follows from the parametric representation of Eq. 49. Numerical examples are provided in Fig. 11.

REMARKS ON THE ANALYSIS

The model treated here adopts the Oseen approximation, does not pursue the details of flow stagnation at the boom, and takes the oil layer to remain coherent. We believe that we have solved the model to the accuracy warranted. In general, pursuing more meticulous

mathematical solution of the above formulation does not seem appropriate without first inquiring into the magnitude of possible modifications owing to turbulent transition; standing waves established by the presence of the towing vessels and the boom; pre-existing waves, currents, and/or winds; and firespread rate. Further work on the containment configuration may consider a model of the boom beyond that of the string idealization adopted here.

One exception to this recommendation concerns the fact that a solution is furnished above for a two-dimensional problem: a one-dimensional or two-dimensional problem often is usefully considered at the outset of almost any combustion-front-propagation investigation. Extension to a three-dimensional description of oil-layer depth during a remediation operation might be usefully undertaken with just the phenomena currently included in the model.

PERTINENT LABORATORY EXPERIMENTS

The experiments to be discussed may all be carried out in a flume, a (modestly) sloped channel into which one can introduce water, a surface layer of oil, and (if desired) a stationary boom past which the liquid may flow (Fig. 12). The capacity to have a finite wind speed w may be noted. Of course, the inlet and outlet may be plugged so that tests without a moving layer are encompassed.

The first, crucial laboratory experiments are those that delineate the amount of burning oil consumed per unit area per time, i.e., the quantity $\dot{m}$, with the units of a speed. The data for $\dot{m}$ should be sought for types of oils of interest and for oil-layer depths of interest, with wind speeds of interest and with extension to oil/water emulsions to simulate some of the consequences of "weathering" [21,22] of spilled oil. While the existence of appreciable data from burning oil films over water sublayers in pools of various data has been noted in the introduction, the desired information cited here appears to go beyond what is available.

The next set of laboratory experiments is transient tests of the flame-propagation speed across the water-supported oil film, for a range of interesting values of each of the above-listed parameters.

If the results continue to support the practicality of the scheme, currently plausible on the basis of a quite limited number of uninstrumented trials at sea, then the next step would be to try to simulate the entire phenomenon in the laboratory; it is this encompassing simulation that is depicted in Fig. 12. Such an inclusive laboratory simulation would entail a moving layer, ignition at time zero, and spread of flame across the oil layer.

The authors are grateful to Howard Baum, David Evans, and Douglas Walton of the Center for Fire Research, National Institute of Standards and Technology, Gaithersburg, MD for many very helpful discussions. They also wish to thank Christine McCourt and Gail Takahashi for the preparation of the manuscript.

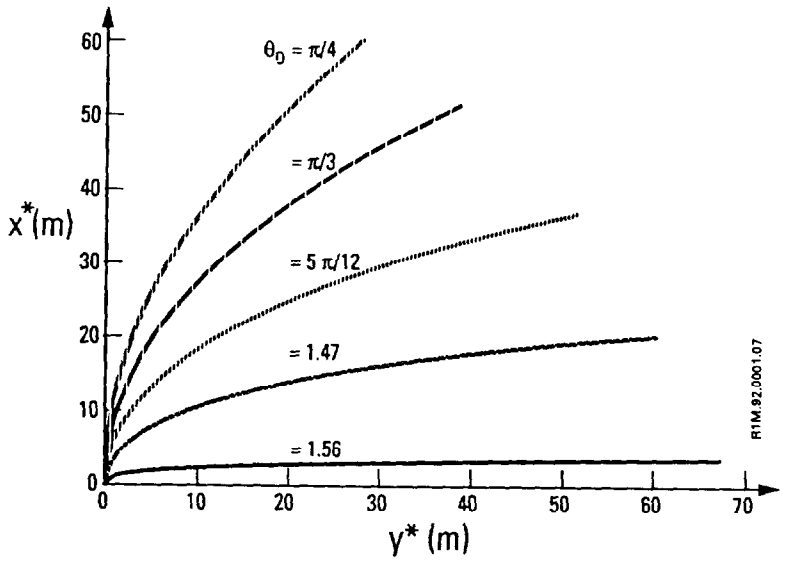

Figure 11. The configuration of half the boom, in terms of the coordinate system introduced in Fig. 8, from Eqs. 47 and 49, for a half-boom length L* = 67.5 m and for various tow angles θ_0. The full boom configuration is implied since the configuration is symmetric about the y* axis.

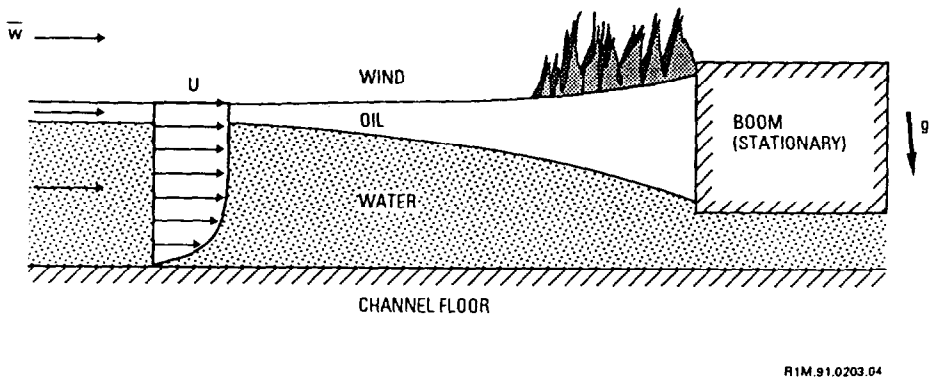

Figure 12. Schematic of a flow-through experiment in a (slightly inclined) channel with a stationary boom, and a burning oil layer at the surface of the water. The wind speed is $\bar{w}$ and the liquid phases move at speed U far from the boom (aside from boundary layers); however, after a fetch, the wind alters the liquid speed from U, as does the approach to the boom.

NOMENCLATURE

C_D	coefficient of drag, defined in Eq. 45
D	drag, [N]
$d(x)$	magnitude of the depth of the oil-water interface below the level of the ambient water surface, [m]
$f(s)$	$M(x)/(Uh_\infty)$
g	magnitude of the gravitational acceleration, [m/s^2]
$H(s)$	$[\eta(x) + d(x)]/h_\infty$
H^*	depth of the wetted part of the boom, [m]
h_∞	ambient thickness of the oil slick, [m]
K	dimensionless parameter defined in Eq. 30
$K(s)$	integrably singular kernel defined above Eq. 36
k	$\rho C_D U^2 H^*/(2T)$, [1/m]
L	magnitude of the value of the x coordinate at which the oil-layer thickness begins to vary from h_∞, [m]
L^*	half the length of the boom, [m]
$M(x)$	$\int_x^0 \dot{m}(\delta)\, d\delta$, [m^2/s]
$\dot{m}$	oil-surface-regression rate, [m/s]
$p(x,y)$	pressure, with datum at the air-oil interface, [Pa]
s	x/L
s^*	distance along the arc of the boom (Fig. 9), [m]
T	tension along the tangent to the boom, [kg/(m s^2)]
t	$s + 1$
U	towing speed, [m/s]
$u(x,y)$	component of velocity in the x direction, [m/s]
$u_1(x)$	$u[x,-d(x)]$, [m/s]
$u^*(x,y)$	$u(x,y) - U$, [m/s]
$v(x,y)$	component of velocity in the y direction, [m/s]

$w(s)$	$u_1(x)/U$
x	horizontal Cartesian coordinate, with origin at the boom, [m]
x^*	Cartesian coordinate defined in Fig. 9, [m]
y	vertical Cartesian coordinate, with origin at the ambient water surface, [m]
y^*	Cartesian coordinate defined in Fig. 9, [m]
ϵ	$(\pi/2) - \theta_0$
ς	Fourier-transform variable, [1/m]
$\eta(x)$	height of the air-oil interface above the ambient water surface, [m]
θ	angle defined in Fig. 9
θ_0	asymptotic value of θ, holding at the end of the boom (Fig. 9)
λ	dimensionless parameter defined in Eq. 30
μ	viscosity of the water, [kg/(m s)]
μ_0	dynamic viscosity of the oil, [kg/(m s)]
ν	μ/ρ, [m^2/s]
ρ	density of the water, [kg/m^3]
σ	density of the oil, [kg/m^3]
$\tau_{xy}(x,y)$	component of the shear-stress tensor, [$kg/(m\ s^2)$]

Superscript

$\bar{}$	Fourier-transformed quantity

REFERENCES

1. U.S. Congress, Office of Technology Assessment, Coping with an Oiled Sea: An Analysis of Oil Spill Response Technologies, Report OTA-BP-O-63, U.S. Government Printing Office, Washington, DC, 1990, pp. 1-26, 51-57.

2. Evans, D. D., "In-Situ Burning of Oil Spills," Alaska Arctic Offshore Oil Spill Response Technology (N. H. Jason, Ed.), Report NIST SP 762, U.S. Government Printing Office, Washington, DC, 1988, pp. 47-95.

3. Evans, D., Mulholland, G., Gross, D., Baum, H., and Saito, K., "Generation and Dispersal of Smoke from Oil Spill Combustion," Proceedings 1989 Oil Spill Conference (Prevention, Behavior, Control, Cleanup), American Petroleum Institute/Environmental Protection Agency/United States Coast Guard, Washington, DC, 1989, pp. 181-185.

4. Evans, D. Walton, W., Baum, H., Lawson R., Rehm, R., Harris, R., Ghoniem, A., and Holland, J., "Measurement of Large-Scale Oil Spill Burns," Proceedings of the Thirteenth Arctic and Marine Oil Spill Program Technical Seminar, Minister of Supply and Services (Cat. No. EN 40-11/5-1990), Canada, 1990, pp. 1-38.

5. Allen, A. A., "Contained Controlled Burning of Spilled Oil During the Exxon Valdez Oil Spill," Proceedings of the Thirteenth Arctic and Marine Oil Spill Program Technical Seminar, Minister of Supply and Services (Cat. No. EN 40-11/5-1990), Canada, 1990, pp. 305-313.

6. Evans, D., Walton, W., Baum, H., Mulholland, G., and Lawson, J., "Smoke Emission from Burning Crude Oil," Proceedings of the Fourteenth Arctic and Marine Oil Spill Program Technical Seminar, Ministry of Supply and Services (Cat. No. EN 40-11/5-1991), Canada, 1991, pp. 421-449.

7. Fingas, M., and Laroche, N., "An Introduction to In-Situ Burning of Oil Spills," Spill Technology Newsletter 15(4):1-11 (December 1990).

8. Benner, Jr., B. A., Bryner, N. P., Wise, S. A., Mulholland, G. W., Lao, R. C., and Fingas, M. F., "Polycyclic Aromatic Hydrocarbon Emissions from the Combustion of Crude Oil on Water," Environ. Sci. Tech. 24:1418-1427 (1990).

9. Mitchell, J. B. A., "Smoke Reduction from Burning Crude Oil Ferrocene and Its Derivatives," Combust. Flame 86:179-184 (1991).

10. Mitchell, J. B. A., "Smoke Reduction from Burning Crude Oil Using Ferrocene and Its Derivatives," Spill Technology Newsletter 15(4):11-20 (December 1990).

11. Fay, J. A., "The Spread of Oil Slicks on a Calm Sea," Oil on the Sea, Plenum, New York, NY, 1969, pp. 53-64.

12. Hoult, D. P., "Oil Spreading on the Sea," Ann. Rev. Fluid Mech. 4:341-368 (1972).

13. Spaulding, M. L., "A State-of-the-Art Review of Oil Spill Trajectory and Fate Modelling," Oil & Chemical Pollution 4:39-55 (1988).

14. Twardus, E. M., and Brzustowski, T. A., "The Burning of Crude Oil Spilled on Water," Archivum Combustionis (Polish Academy of Sciences) 1 (1/2):49-60 (1981).

15. Brzustowski, T. A., and Twardus, E. M., "A Study of the Burning of a Slick of Crude Oil on Water," Nineteenth Symposium (International) on Combustion, Combustion Institute, Pittsburgh, 1982, pp. 847-854.

16. Brzustowski, T. A., "A Study of the Burning of Unconfined Oil Slicks," Trans. Canadian Soc. Mech. Engineers 9:192-199 (1985).

17. Alramadhan, M. A., Arpaci, V. S., and Selamet, A., "Radiation Affected Liquid Fuel Burning on Water," Combust. Sci. and Tech. 72:233-253 (1990).

18. Lewis, J. A., and Carrier, G. F., "Some Remarks on the Flat Plate Boundary Layer," Quart. Appl. Math. 7:228-234 (1949).

19. Symon, K. R., Mechanics, Addison-Wesley, Reading, MA, 1953, pp. 205-207.

20. Schlichting, H., Boundary-Layer Theory, 7th Ed., McGraw-Hill, New York, 1979, pp. 15-19.

21. Daling,, P. S., Brandvik, P. J., Mackay, D., and Johansen, O., "Characterization of Crude Oils for Environmental Purposes," Proceedings of the Thirteenth Arctic and Marine Oil Spill Program Technical Seminar, Minister of Supply and Services (Cat. No. EN 40-11/5-1990), Canada, 1990, pp. 119-138.

22. Holloway, M., and Horgan, J., "Soiled Shores," Scientific Amer. 265:102-116 (1991).